2025 IEEE/SICE International Symposium on System Integration (SII)
January 21-24, 2025, Munich, Germany

Improving Back-drivability of Robot Joint by Reducing Reflected Inertia Using Multi-motor System

Zexin Shan[1], Mitsuru Endo[1], Yukio Tsutsui[2,3], and Shimpei Tanaka[3]

Abstract— **Enhancing back-drivability in robot joints is crucial for safe and effective physical human-robot interaction (pHRI). This paper presents a novel approach to improve back-drivability by reducing reflected inertia through a multi-motor system (MMS). Unlike traditional high-ratio gearboxes, which amplify motor inertia and reduce efficiency, the MMS distributes torque across multiple motors, allowing for lower gear ratios and less reflected inertia. We developed an optimization model considering motor selection, gear ratios, and gear stages to minimize reflected inertia while meeting load and geometric constraints. A case study on an industrial robot's shoulder joint demonstrates an 88.84% reduction in reflected inertia using the proposed MMS compared to a conventional single-motor system. The findings suggest that multi-motor systems can significantly reduce reflected inertia, improving back-drivability in robot joints for safer and more efficient pHRI.**

I. INTRODUCTION

Physical human-robot interaction (pHRI) is increasingly desirable in robotics in order to realize harmonic co-existence between humans and robots. For example, some wearable robots are designed to assist the human in daily life, such as exoskeletons for older or disabled people [1], service robots are designed to assist in cleaning or object transportation [2], and collaborative robots are designed to complete tasks with the human in the industrial environment [3]. The applications of these robots involve frequent bi-directional physical interactions between humans and robots. A key feature called back-drivability is required to ensure the safety and user-friendliness of the robots in pHRI [4].

Back-drivability characterizes the robot's ability to be moved by an external force, like human force. To be more specific, the robot should be able to be back-driven by humans with low resistance. Many prior studies have been conducted to investigate the methods to realize high back-drivability. Methods are generally categorized into two types: powered back-drivability and unpowered back-drivability [5].

Powered back-drivability is achieved by employing advanced control algorithms and sensors to detect the external force and actively generate appropriate torque to reversely drive the robot. The most common method is the one applying the series elastic actuator (SEA) [6], [7], [8]. An elastic element is placed between the gearbox output and the load. Therefore, the contact force from the load can be determined by measuring the displacement of the elastic element by sensors, allowing precise force control. However, it has worse precision in position control. There are also studies using different sensing methods, like obtaining information from a load-side encoder to implement back-driving position control [9]. As we can see, powered back-drivability may be effective but highly relying on the control systems and the sensors. The control band and the sensor band limit its real-world performance. More importantly, pHRI safety is not guaranteed during sensor malfunction, making it not intrinsically safe.

In contrast, unpowered or passive back-drivability is achieved by developing mechanically safe robots, which allows the robots to be passively back-drivable without elastic elements and active actuation by control systems and sensors. Two main contributing factors to passive back-drivability are the power transmission efficiency of the robot joint and the reflected motor inertia. Therefore, they lead to two main research directions to improve passive back-drivability: increasing the power transmission efficiency and reducing the reflected motor inertia.

The efficiency is mainly determined by the friction between the gearbox's meshing gears. A single motor with a high-reduction-ratio gearbox is usually used in the robot joint to achieve the required torque and, thus, increase the torque density. However, the friction generally increases with the gear ratio, leading to decreased power transmission efficiency. The strain wave gearbox and the RV reducers are the most common high-ratio gearboxes used in the robot joint because they can achieve a high gear ratio with a compact size. However, the high reduction ratio and their unique structures contribute to low efficiency [10], [11]. To solve this problem, Ishida and Takanishi proposed a design method for a robot actuator with high back-drivability, which mainly involves reducing the reduction ratio and changing the gear teeth profile to reduce friction [4]. Kobuse and Fujimoto proposed a method to maximize efficiency of a planetary gearbox with a high reduction ratio by optimizing gear teeth profile-shift coefficients [12]. Later, Matsuki et al. optimized both the teeth numbers and the teeth profile-shift coefficients of the 3K planetary gearbox to maximize the efficiency [13]. Most of these studies focus on the optimization of the gear teeth profile to reduce the friction, but the gear ratio is still high, which may still maintain a high reflected inertia of the motor.

Let G_t denote the total reduction ratio of a gearbox. The reflected motor inertia to the joint output shaft is scaled by

*This work was supported by Yaskawa Electric Corp.

[1]Z. Shan, and M. Endo are with the Faculty of Mechanical Engineering, Institute of Science Tokyo, Meguro, Tokyo 152-8550, Japan shan.z.14bc@m.isct.ac.jp

[2]Y. Tsutsui is with the Faculty of Electrical Engineering, Institute of Science Tokyo, Meguro, Tokyo 152-8550, Japan tsutsui.y.ad@m.titech.ac.jp

[3]Y. Tsutsui and S. Tanaka are with the Yaskawa Electric Corporation, 2-1 Kurosakishiroishi, Yahatanishi-ku, Kitakyushu 806-0004 Japan

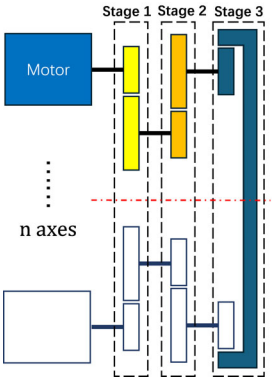

Fig. 1: Conceptual figure of multi-motor system

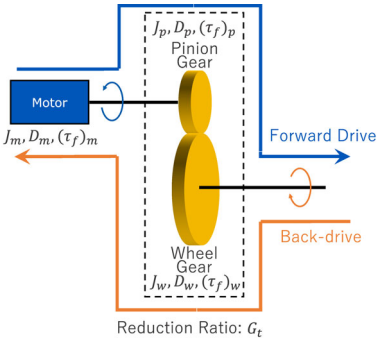

Fig. 2: Schematic of a simple robot joint

the factor of the square reduction ratio ($\propto G_t^2$). Even though the original motor rotational inertia is very small, its effect on back-driving the joint can immediately be amplified by a considerable number, as mentioned in [14]. Related studies to tackle it are focusing more on using direct-drive (DD) or quasi-direct-drive (QDD) that eliminated the transmission or used a low-ratio transmission, respectively, for the exoskeletons and legged robots. Wang et al. proposed a back-drivable knee exoskeleton that has a QDD transmission to keep a low reflected inertia [15]. Kenneally et al. proposed a method to design legged robots using DD [16]. Seok et al. designed a legged robot called the MIT cheetah robot with a QDD transmission [17]. While using DD and QDD can effectively reduce the reflected inertia, their applications are still limited to low-torque robots, and they fail to meet the demands of high-torque industrial robots without significantly increasing motor size, which is impractical for joint integration. This issue sparks the idea of using a multi-motor system (MMS) as a different way to increase the actuator torque to reduce the required gear ratio and, thus, the reflected motor inertia. Previous research has largely overlooked the use of MMS in robotic joints due to the prevailing reliance on DD and QDD systems.

Some prior studies related to MMS have been conducted in various fields. The purposes are to increase the power of the heavy-duty or automotive system [18], [19], [20], to optimize the energy allocation [21], [22], or to improve the control performance of the system [23]. Saito et al. proposed a lightweight redundant joint with multiple motors, but it aims to reduce the weight of wearable robots that only require small torque [24]. Unlike automobile systems, which prioritize power output, or wearable robots, which focus on compactness and low weight, industrial robot joints demand a balance between high torque, compact design, and mechanical efficiency. These differences necessitate an optimal design approach uniquely suited to robot joints.

Herein, we investigate the possibility of optimizing the reflected inertia of the robot joint by using a MMS. This study bridges the gap in research by introducing an optimization framework that adapts MMS principles to robotic joints. By addressing load and geometric constraints, the proposed approach enables significant reductions in reflected inertia, which are critical for improving back-drivability in high-torque industrial robots. The conceptual figure of such a system with three gear stages is illustrated in Fig. 1. The system consists of multiple motors and a multi-stage parallel shaft gear train, where the selected motor model, the number of motor axes, the number of gear stages, and the gear ratio of each stage become the factors altering the reflected inertia. Each motor axis applies the simple gear train with a pinion and a wheel for each stage to the common ring gear. Positions of axes are uniformly distributed around the ring gear to ensure the torque is evenly distributed. We realize there are other ways of arranging the motors and gears, but we choose this arrangement for the sake of simplicity and uniformity of the torque distribution. It enhances the system's robustness and reliability. The optimization method and a case study are presented to demonstrate the effectiveness of the MMS in reducing the reflected inertia of the robot joint.

II. REFLECTED INERTIA IN ROBOT JOINT

To discuss the resistance to back-driving joints, we need to look at the motion equation of the robot's joint. Fig. 2 shows the schematic of a simple robot joint, which consists of a motor and a gear train. Since the damping of the wheel and the pinion is usually small compared to the inertia and the friction torque of the gear train, we neglect the damping terms. The motion equation for back-driving the joint is given by:

$$T_{BD} = J_w \ddot{\theta}_L + (J_p + J_m)\ddot{\theta}_m + T_{f,g} \tag{1}$$

where T_{BD} is the torque required to back-drive the joint, J_w and J_p are the inertia of the wheel and the pinion, respectively, J_m is the inertia of the motor, $T_{f,g}$ is the friction torque of the gear train, θ_L is the angle of the wheel and the load, and θ_m is the angle of the pinion and the motor.

Thus, the torque required to back-drive the joint is mainly determined by the inertia of the wheel and the pinion, as well as the friction torque of the gear train. We can transform the system into a lumped system with the reflected inertia and the friction to the joint output shaft, as shown in Fig. 3.

As viewed from the output shaft of the lumped system, the motion equation for back-driving the joint is now given by:

$$T_{BD} = \left[J_w + G_t^2(J_p + J_m)\right]\ddot{\theta}_L + G_t T_{f,r} \tag{2}$$

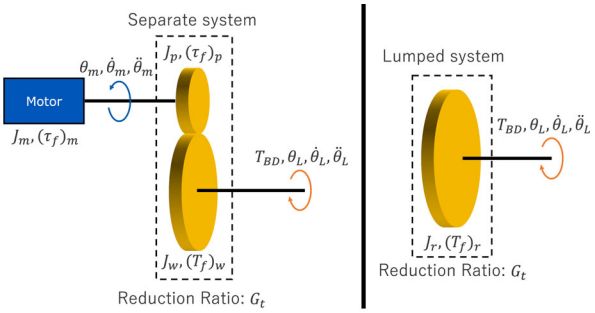

Fig. 3: Lumped system of a robot's joint

where G_t is the total gear ratio of the gear train, and $T_{f,r}$ is the reflected friction of the joint. The term $J_{r,t} = J_w + G_t^2(J_p + J_m)$ is called the total reflected inertia of the joint, which is the sum of the wheel's inertia and the gear train's component. The term $G_t T_{f,r}$ is called the reflected friction of the joint, which is the friction torque of the gear train amplified by the gear ratio. Thus, in the case of a robot's joint using a high-ratio gear train, the inertia and the friction of the gear train will have a significant impact on the resistance to back-driving.

III. REFLECTED INERTIA OF MULTI-MOTOR SYSTEM

The total reflected inertia, $J_{r,t}$, of the multi-motor system (MMS) is the sum of the reflected inertia of each motor and the component of the gear train. The gear train is a multi-motor multi-stage parallel shaft gear train with n driving axes for n motors, which is connected to a common ring gear and thus the common output shaft.

The total gear ratio of the gear train is G_t, and the gear ratio of each stage is G_i, where $i = 1, 2, \ldots, a$ and a is the number of stages in the gear train. In this study, we only investigate up to three stages ($a \in [1,2,3]$) because too many stages make the system too complex to analyze, and the gear train's efficiency will be decreased dramatically. Therefore, the contents of the following sections are based on three topologies of MMS: single-stage, dual-stage, and triple-stage.

The gear train is assumed to use identical motors for the sake of simplicity, but the gear ratio of each stage can be different for easier arrangement of the gears' sizes and positions. The inertia of each motor is J_m. The reflected inertia of all motors ($J_{r,m}$) is given by:

$$J_{r,m} = nJ_mG_t^2 \tag{3}$$

where J_m is the inertia of the i^{th} motor, G_t is the total gear ratio of the gear train, and n is the number of axes.

Thus, for MMS with a stages, a general formula for the reflected inertia of the gear train $(J_{r,g})_a$ is given by:

$$(J_{r,g})_a = n\sum_{i=1}^{a-1}\left[(J_{pi}G_i^2 + J_{wi})\prod_{j=i+1}^{a} G_j^2\right] + nJ_{pa}G_a^2 + J_{ring} \tag{4}$$

where J_{pi} and J_{wi} are the inertia of the pinions and the wheels of the i^{th} stage, respectively. J_{pa} is the inertia of the pinion of the a^{th} stage, and J_{ring} is the inertia of the ring gear.

Assuming all the pinions and wheels are cylindrical, the inertia of the pinions, the wheels and the ring can be calculated by:

$$J_{pi} = \frac{1}{32}\rho\pi b d_{pi}^4 \tag{5}$$

$$J_{wi} = \frac{1}{32}\rho\pi b d_{wi}^4 \tag{6}$$

$$J_{ring} = \frac{1}{32}\rho\pi b\left[(d_{inner} + 2t_R)^4 - d_{inner}^4\right] \tag{7}$$

where ρ is the density of the material, b is the face width of the pinion and the wheel, d_{pi} and d_{wi} are the pitch diameter of the pinion and the wheel of the i-th stage, respectively, d_{inner} is the inner diameter of the ring gear, and t_R is the rim thickness of the ring gear.

Also, the relationship between the pitch diameter and the teeth number of the pinion, the wheel and the ring is given by:

$$d_{pi} = z_{pi}m_{pi} \tag{8}$$

$$d_{wi} = z_{wi}m_{wi} = z_{pi}G_i m_{pi} \tag{9}$$

$$d_{inner} = z_{ring}m_{ring} = z_{pa}G_a m_{pa} \tag{10}$$

where z_{pi} and z_{wi} are the teeth number of the pinion and the wheel of the i-th stage, respectively, z_{ring} is the teeth number of the ring gear, m_{pi} and m_{wi} are the module of the pinion and the wheel of the i-th stage, respectively, m_{ring} is the module of the ring gear.

Since we wish to have a minimal system size, we will select the smallest available gear size for all pinion gears in the gear train. Now, substituting Eq. (5) and Eq. (8) into Eq. (4) and simplifying, we get:

$$(J_{r,g})_a = \frac{\rho\pi b z_p^4 m^4}{32}\left\{n\sum_{i=1}^{a-1}\left[G_i(G_i+1)\prod_{j=i+1}^{a}G_j^2\right] + G_a^4\right\} + \frac{\rho\pi b}{32}\left[(z_p m G_a + 2t_R)^4 - (z_p m G_a)^4\right] \tag{11}$$

The total reflected inertia of the multi-motor system is the sum of Eqns. (3) and (11):

$$\begin{aligned} J_{r,t} &= J_{r,m} + J_{r,g} \\ &= nJ_mG_t^2 + \frac{\rho\pi b z_p^4 m^4}{32}\left\{n\sum_{i=1}^{a-1}\left[G_i^2(G_i^2+1)\prod_{j=i+1}^{a}G_j^2\right] + G_a^4\right\} \\ &\quad + \frac{\rho\pi b}{32}\left[(z_p m G_a + 2t_R)^4 - (z_p m G_a)^4\right] \end{aligned} \tag{12}$$

where G_t is the total gear ratio that equals the product of the gear ratios of each stage ($G_t = G_1G_2G_3\ldots G_a$).

The known parameters in Eq. (12) are the density of the material ρ, the face width of the pinion and the wheel b, the teeth number of the pinion z_p, the module of the pinion and the wheel m, and the ring gear's rim thickness t_R. Therefore, it is a function of the inertia of each motor J_m, the gear ratio of each stage $\overline{G} = [G_1, G_2, \ldots G_a] \in Z^a$, the number of stages a, and the number of axes n.

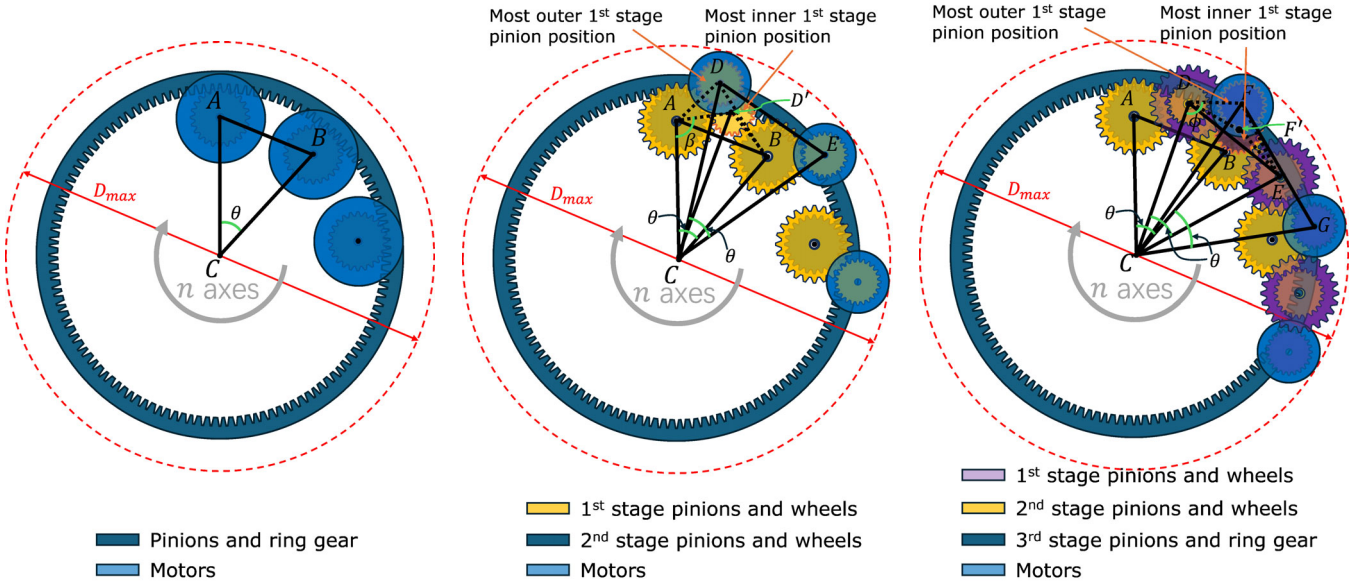

(a) Single-stage MMS (b) Dual-stage MMS (c) Triple-stage MMS

Fig. 4: Geometric constraints of three topologies of MMS

IV. CONSTRAINTS

The constraints of the load and the geometry should be considered to ensure the robot joint can operate properly.

A. Load Constraint

The load constraint is to ensure the joint can provide the required torque to the load when forward driving. The load constraint is given by:

$$h(\overline{G}, T_m, n) = T_{load} - nT_m \prod_{i=1}^{a} G_i \quad \text{where } G_i \in \overline{G} \tag{13}$$

where T_{load} is the required torque to the load, T_m is the rated torque of the motor, and n is the number of axes.

B. Geometric Constraints

The geometric constraints ensure that all the gears and motors can be installed inside the limited space of the robot joint without interfering with each other. Constraints for each MMS topology should be discussed separately. Moreover, starting from the last stage to the first stage is better since all axes mesh with the common ring gear.

1) If Single-Stage MMS: Based on Fig. 4a, the constraint to avoid interference between axes' pinions and between axes' motors are given by:

$$g_1 = d_p + S_{CLR} - L_{AB} < 0 \tag{14}$$

$$g_2 = d_m + S_{CLR} - L_{AB} < 0 \tag{15}$$

$$\text{where} \quad L_{AB} = L_{AC}\sqrt{2(1-\cos\theta)}$$

$$L_{AC} = \frac{d_{inner} - d_p}{2}, \quad \theta = \frac{2\pi}{n}$$

where S_{CLR} is the designer-specified minimum clearance between any two components (gears or motors) in the joint. L_{AB} and L_{AC} are the lengths of the line segments AB and AC in Fig. 4a, respectively. The same notation method is applied to other line segments in the following constraints.

The constraint to avoid exceeding the maximum joint space is given by:

$$g_3 = d_{inner} + d_p - d_m - D_{max} < 0 \tag{16}$$

where D_{max} is the specified maximum diameter of the joint, and d_m is the diameter of the motor.

2) If Dual-Stage MMS: From Fig. 4b, for anti-interference, we do not need to consider the pinions of the final stage, because their diameters are smaller than the coaxial 2nd stage wheels. Following the same process as the single-stage MMS, constraints to avoid interference between axes' wheels and between axes' motors are given by:

$$g_4 = d_{w1} + S_{CLR} - L_{AB} < 0 \tag{17}$$

$$g_5 = d_p + S_{CLR} - L_{DE} < 0 \quad (\text{if } d_p > d_m) \tag{18}$$

$$g_6 = d_m + S_{CLR} - L_{DE} < 0 \quad (\text{if } d_p < d_m) \tag{19}$$

$$\text{where} \quad L_{AB} = L_{AC}\sqrt{2(1-\cos\theta)}, \; L_{AC} = \frac{d_{inner} - d_p}{2}$$

$$L_{DE} = L_{CD}\sqrt{2(1-\cos\theta)}$$

$$\text{if } d_p > d_m: \quad L_{CD} = \frac{D_{max} - d_p}{2}$$

$$\text{if } d_p < d_m: \quad L_{CD} = \frac{D_{max} - d_m}{2}$$

Additionally, the 1st stage pinion may also interfere with the wheels of the neighboring axes. If the clearance space between the neighboring wheels is smaller than the diameter of the pinion, interference will occur. Thus, another constraint

to avoid this is derived by:

$$g_7 = L_{CD'} - L_{CD} < 0 \quad (\text{if } L_{AB} < d_{w1} + d_p + S_{CLR}) \quad (20)$$
$$\text{where } L_{CD'} = \sqrt{(L_{AC})^2 + (L_{AD'})^2 - 2(L_{AC})(L_{AD'})\cos\beta}$$
$$\beta = \cos^{-1}\left[\frac{(L_{AB})^2 + (L_{AD'})^2 - (L_{BD'})^2}{2(L_{AB})(L_{AD'})}\right] + \frac{\pi - \frac{2\pi}{n}}{2}$$
$$L_{AD'} = \frac{d_{w1} + d_p}{2}, \; L_{BD'} = \frac{d_{w1} + d_p}{2} + S_{CLR}$$

where $L_{CD'}$ refers to the lower bound of the distance between the 1st stage pinions' center and the joint center (indicated as the most inner 1st stage pinion position in Fig. 4b). Note that the most outer 1st stage pinion position determined by the pinion's or motor's diameter is used to calculate L_{CD} in the constraint g_7 to deal with the worst-case scenario. The same method is applied to similar constraints for the triple-stage MMS later.

The constraint to prevent 1st stage wheels from exceeding the maximum joint space is:

$$g_8 = d_{inner} + d_{w1} - d_p - D_{max} < 0 \quad (21)$$

To prevent motors from exceeding the maximum joint space, the constraint is:

$$g_9 = L_{CD} + \frac{d_m}{2} - \frac{D_{max}}{2} < 0 \quad (22)$$

3) If Triple-Stage MMS: Triple-stage MMS is based on the dual-stage one, so the constraints g_4, g_5, g_7, and g_8 should also be included. To avoid redundancy, we do not repeat them here, but we need to change all d_{w1} to d_{w2} due to the additional stage.

Based on Fig. 4c, the constraints to avoid interference between axes' wheels and between axes' motors is:

$$g_{10} = d_{w1} + S_{CLR} - L_{DE} < 0 \quad (23)$$
$$\text{where} \quad L_{DE} = L_{CD}\sqrt{2(1 - \cos\theta)}$$

Similarly, the 1st stage pinions may interfere with the wheels of the neighboring axes. The constraint to avoid this is given by:

$$g_{11} = L_{CF'} - L_{CF} < 0 \quad (\text{if } L_{DE} < d_{w1} + d_p + S_{CLR}) \quad (24)$$
$$\text{where } L_{CF'} = \sqrt{(L_{DF'})^2 + (L_{CD})^2 - 2(L_{CD})(L_{DF'})\cos\phi}$$
$$\phi = \cos^{-1}\left[\frac{(L_{DE})^2 + (L_{DF'})^2 - (L_{EF'})^2}{2(L_{DE})(L_{DF'})}\right] + \frac{\pi - \frac{2\pi}{n}}{2}$$
$$L_{CF} = \frac{D_{max} - d_m}{2}, \quad L_{CD} = \frac{D_{max} - d_{w1}}{2}$$
$$L_{DF'} = \frac{d_{w1} + d_p}{2}, \quad L_{EF'} = \frac{d_{w1} + d_p}{2} + S_{CLR}$$

To prevent motors from exceeding the maximum joint space, the constraint is:

$$g_{12} = L_{CF} + \frac{d_m}{2} - \frac{D_{max}}{2} < 0 \quad (25)$$

V. OPTIMIZATION OF REFLECTED INERTIA

After we have formulated the total reflected inertia of the multi-motor system, the load constraint, and the geometric constraints, we can now optimize the reflected inertia of the robot joint.

A. Optimization Problem

The optimization problem is formulated using the total reflected inertia of the robot joint as the objective function and all constraints:

$$\begin{aligned} \underset{a,n,J_m,\overline{G}}{\text{minimize}} \quad & J_{r,t} \\ \text{subject to} \quad & h = 0 \\ & g_i < 0, \; i = 1,2,\ldots,12 \end{aligned} \quad (26)$$

B. Optimization Algorithm

The optimization algorithm is a nested DIRECT algorithm based on the nested loops and the DIRECT method [25]. It is shown in Algorithm 1.

There are three nested loops for the number of stages a, the number of axes n, and the motor inertia J_m. For each combination of (a,n,J_m), the DIRECT method is used to optimize the gear ratio G_i of each stage. The optimal combination of $(a,n,J_m,\overline{G})$ is determined by minimizing the total reflected inertia of the robot joint.

Algorithm 1 Nested DIRECT Method

```
Input: Objective function J_{r,t}(a, n, J_m, G)
Output: Optimal values a*, n*, J_m*, G*
for each a ∈ {1,2,3} do
    for each n ∈ {1,2,...,8} do
        for each J_m in the motor catalog do
            Use the DIRECT method to optimize f(a,n,J_m,G) with respect to G
        end for
        Record the optimal G and the corresponding objective function value
    end for
end for
Determine (a*, n*, J_m*, G*) that minimizes J_{r,t}
```

VI. CASE STUDY

To demonstrate the effectiveness of the multi-motor system in reducing the reflected inertia of the robot joint, a case study is conducted.

A. Reference Robot Joint

The shoulder joint of Universal Robots UR10e is selected as the reference robot joint. Since we do not have the detailed information of the UR10e, we use its specifications from the datasheet [26] and the worst-case scenario to estimate the maximum required dynamic torque. The scenario is that the UR10e accelerates the maximum payload at an assumed maximum acceleration when the robot is stretched out horizontally. Some specifications, the estimated maximum

TABLE I: Reference Robot Joint Specifications

Specifications	Value
Maximum Payload [kg]	12.5
Assumed Maximum Acceleration [rad/s^2]	4.0
Maximum Speed [rad/s]	2.09
Estimated Required Dynamic Torque [Nm]	196
Selected Motor	Maxon EC 90 flat 400 W
Selected Gearbox	Harmonic Drive SHG-25-160-2UH
Motor Inertia [kgm^2]	0.000476
Motor Rated Torque [Nm]	1.27
Gear Ratio	160
Gearbox Moment of Inertia [kgm^2]	0.000109
Reference Reflected Inertia [kgm^2]	12.19

TABLE II: Parameters for Optimization

Parameters	Value
Density of Gear Material [kg/m^3]	2800
Gear Module [m]	0.001
Gear Facewidth [m]	0.006
Ring Gear Rim Thickness [m]	0.008
Pinion Gear Teeth	14
Maximum Allowable System Diameter [m]	0.2
Maximum Allowable System Length [m]	0.25

required torque, and the selected motor and gearbox based on the estimated torque, and the reference reflected inertia are shown in TABLE I.

B. Optimization Implementation

The optimal design of the multi-motor system with a similar torque capacity as the reference robot joint is obtained using the nested DIRECT method. The motor catalog is selected from the Maxon RE motor catalog [27].

1) Given Parameters: Some parameters are specified for the optimization, as shown in TABLE II. The maximum allowable system diameter and length should be based on the reference robot joint's specifications. However, UR10e's detailed information is not available, so by inspecting the Spec. Sheet of UR10e, the maximum allowable system diameter and length are estimated to be 0.2 m and 0.25 m, respectively. The gear material is set to be Aluminum 7075-T6, and the gear module is set to be 0.001 m.

2) Optimal Design: The optimal design values that minimize the total reflected inertia of the robot joint are shown in TABLE III. To be more realistic, the bending stress and

TABLE III: Optimal Design of Multi-Motor System

Parameters	Value
System Diameter [m]	0.198
System Length [m]	0.231
Number of Stages	3
Number of Axes	5
Motor Model	Maxon RE 65 70V 250W
Motor Inertia [kgm^2]	0.000134
Gear Ratio of Each Stage	[2.79, 2.79, 5.79]
Total Reflected Inertia [kgm^2]	1.37
Reflected Inertia Change	-88.7%

TABLE IV: Gear Parameters of the Modified Optimal Design

Parameters	Value
Gear Material	Aluminum 7075-T6
Gear Module [m]	0.001
Ring Gear Rim Thickness [m]	0.008
1st Stage Facewidth	0.01
2nd Stage Facewidth	0.026
3rd Stage Facewidth	0.028
1st Stage Teeth (Pinion, Wheel)	(20, 56)
2nd Stage Teeth (Pinion, Wheel)	(20, 56)
3rd Stage Teeth (Pinion, Wheel)	(30, 174)

the surface pressure stress of the gears should be checked to ensure they can withstand the required torque.

Using the Lewis Bending Strength Equation [28], the bending stress of the gears can be approximated. The bending stress of the gears in stage 2 and stage 3 exceeds the yielding strength (480 MPa) of the gear material. Regarding the surface pressure stress, we can use the Hertzian contact stress equation [28] to calculate the surface pressure stress of the material. The surface pressure stress of the gears in all three stages exceeds the maximum compression stress (690 MPa) of the gear material. Some modifications are made to the gear dimensions (teeth numbers and Facewidths) of the current optimal design to reduce the bending and surface pressure stress. The CAD model of the modified optimal design is shown in Fig. 5. The specifications of the modified optimal design are shown in TABLE III, and the detailed gear parameters are shown in TABLE IV.

3) Preliminary Simulation: To verify the effectiveness of the optimal design, a preliminary simulation to compare the back-driving acceleration of the reference robot joint and the optimal multi-motor system is conducted. The simulation is done in MATLAB/Simulink with the Simscape Driveline toolbox. The optimal MMS is modeled in Simscape Driveline using multiple simple gear blocks. Simscape inertia blocks are added to represent the inertia of the gears and the motors.

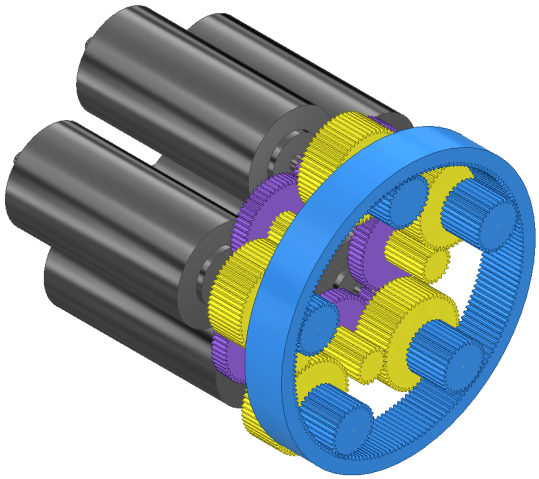

Fig. 5: CAD model of the modified MMS optimal design

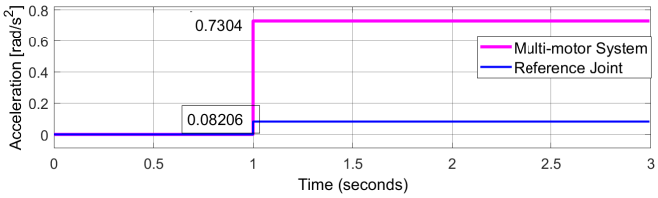

Fig. 6: Simulation comparison of back-driving acceleration

The reference robot joint is modeled using the same method. A step input of 1 Nm is applied to both joints, and the back-driving acceleration of both joints is recorded. The simulation results are shown in Fig. 6.

VII. DISCUSSION

A. Effectiveness of Multi-Motor System

The optimal design of the multi-motor system can reduce the total reflected inertia of the robot joint by 88.7% compared to the reference robot joint. The preliminary simulation results show that the back-driving acceleration of the optimal multi-motor system is significantly higher than the reference robot joint for a 1 Nm back-driving torque (0.7304 m/s^2 >> 0.08206 m/s^2). This indicates that the optimal multi-motor system can provide better back-driving performance than the reference robot joint.

B. Effectiveness of Optimization

Since this paper also focuses on the optimization method, the effectiveness of the optimization method should be verified. An example of designing a multi-motor system with the same torque capacity without optimization is conducted to compare the reflected inertia reduction with the optimal design. The specifications of the non-optimized design are shown in TABLE V. The total reflected inertia of the non-optimized design is 11.68 kgm^2, which is only 8.1% lower than the reference robot joint. The approximate reflected inertia reduction of the non-optimized design is 3.61 kgm^2, which is 70.4% lower than the reference robot joint, but 2.6 times higher than the optimal design. This indicates that the optimization method can further reduce the reflected inertia of the robot joint.

TABLE V: Non-Optimized Design of Multi-Motor System

Parameters	Value
Number of Stages	3
Number of Axes	7
Motor Model	Maxon RE 40 48V 150W
Motor Inertia [kgm^2]	0.0000137
Gear Ratio of Each Stage	[4.17, 4.17, 8.39]
Total Reflected Inertia [kgm^2]	3.61
Reflected Inertia Change	-70.4%

C. Limitations

1) Increase in Weight: The optimal multi-motor system designed by the proposed method does not consider the weight of the robot joint. The additional motors and gears will increase the weight of the robot joint, which may affect the robot's overall performance.

2) Friction: The proposed method does not consider the friction of the gear train. The friction, as another source of resistance to back-driving, will affect the back-driving performance of the robot joint. The additional motors and gears may increase the friction of the robot joint.

3) Efficiency: The proposed method does not include the efficiency in the optimization. The efficiency of the gear train that is affected by multiple factors, will affect the energy consumption of the robot joint. The additional motors and gears may reduce the efficiency of the robot joint, which may require further optimization.

4) Optimization Excluding Stress Analysis: In the proposed method, the optimization is conducted without considering the stress analysis of the gears. Therefore, the bending and surface pressure stress of the gears are manually checked after the optimization, and the gear dimensions are modified to reduce the stress. A more integrated optimization method that considers the stress analysis of the gears should be developed.

5) Motor Cogging Torque: Motor cogging torque is the torque ripple produced by the interaction between the permanent magnets and the stator teeth of the motor. The motor cogging torque is another source of resistance to back-driving. The cogging torque effect of the additional motors has not been investigated in this study.

6) Control System Design: For a well-functioning multi-motor system, a control system that can synchronize the motors and distribute the load among the motors is required, which presents a significant challenge. Some control strategies, such as the distributed cooperative control strategy [23], can be considered.

D. Future Work

To address the limitations of the proposed method, the following future work is suggested:

- Develop a dual-objective optimization method that considers the total reflected inertia and the weight of the robot joint.
- Investigate the friction and efficiency of the gear train and optimize the gear design to reduce the friction and improve the efficiency.
- Include the stress analysis of the gears in the optimization to ensure the gears can withstand the required torque.
- Investigate the motor cogging torque effect and take it as an additional criterion in the optimization.
- Develop a control system that can synchronize the motors and distribute the load among the motors.
- Investigate alternative MMS layouts, such as dividing motors both sides of the ring gear, which increases available space while maintaining structural benefits.
- Consider a broader range of motors beyond the Maxon RE motor series to provide more options for the optimal design.
- Conduct experiments to validate the effectiveness of the optimal multi-motor system in a real robot joint.

VIII. CONCLUSION

In this paper, a novel method to optimize the reflected inertia of a robot joint using a multi-motor system is proposed. The method formulates the total reflected inertia of the robot joint, the load constraint, and the geometric constraints. The optimization problem is formulated using the total reflected inertia as the objective function and the constraints. The nested DIRECT method is used to solve the optimization problem. A case study is conducted to demonstrate the effectiveness of the multi-motor system in reducing the reflected inertia of the robot joint, showing an 88.7% reduction in the total reflected inertia compared to the reference robot joint.

REFERENCES

[1] H. Zhu, C. Nesler, N. Divekar, V. Peddinti, and R. D. Gregg, "Design principles for compact, backdrivable actuation in partial-assist powered knee orthoses," IEEE ASME Trans. Mechatron., vol. 26, no. 6, pp. 3104–3115, 2021.

[2] A.-H. Chiang and S. Trimi, "Impacts of service robots on service quality," Serv. Bus., vol. 14, no. 3, pp. 439–459, 2020.

[3] A. Cherubini, R. Passama, A. Crosnier, A. Lasnier, and P. Fraisse, "Collaborative manufacturing with physical human–robot interaction," Robot. Comput. Integr. Manuf., vol. 40, pp. 1–13, 2016.

[4] T. Ishida and A. Takanishi, "A robot actuator development with high backdrivability," in 2006 IEEE Conference on Robotics, Automation and Mechatronics, 2006.

[5] Q. Du, T. Zhang, G. Yang, C.-Y. Chen, W. Wang, and C. Zhang, "A review of powered backdrivability of robot actuators for human-robot interaction," in 2021 IEEE 16th Conference on Industrial Electronics and Applications (ICIEA), 2021.

[6] G. A. Pratt and M. M. Williamson, "Series elastic actuators," in Proceedings 1995 IEEE/RSJ International Conference on Intelligent Robots and Systems. Human Robot Interaction and Cooperative Robots, 2002.

[7] M. Zinn, O. Khatib, B. Roth, and J. K. Salisbury, "Playing it safe," IEEE Robot. Autom. Mag., vol. 11, no. 2, pp. 12–21, 2004.

[8] M. Laffranchi, N. Tsagarakis, and D. G. Caldwell, "A compact compliant actuator (CompActTM) with variable physical damping," in 2011 IEEE International Conference on Robotics and Automation, 2011.

[9] S. Yamada and H. Fujimoto, "Position-based high backdrivable control using load-side encoder and backlash," IEEJ J. Ind. Appl., vol. 10, no. 2, pp. 142–152, 2021.

[10] J. W. Sensinger and J. H. Lipsey, "Cycloid vs. harmonic drives for use in high ratio, single stage robotic transmissions," in 2012 IEEE International Conference on Robotics and Automation, 2012.

[11] J. W. Sensinger, "Efficiency of high-sensitivity gear trains, such as cycloid drives," J. Mech. Des. N. Y., vol. 135, no. 7, p. 071006, 2013.

[12] D. Kobuse and Y. Fujimoto, "Efficiency optimization of high-reduction-ratio planetary gears for very high power density actuators," in 2016 IEEE 25th International Symposium on Industrial Electronics (ISIE), 2016.

[13] H. Matsuki, K. Nagano, and Y. Fujimoto, "Bilateral drive gear—A highly backdrivable reduction gearbox for robotic actuators," IEEE ASME Trans. Mechatron., vol. 24, no. 6, pp. 2661–2673, 2019.

[14] P. Lopez Garcia, E. Saerens, S. Crispel, A. Varadharajan, D. Lefeber, and T. Verstraten, "Factors influencing actuator's backdrivability in human-centered robotics," MATEC Web Conf., vol. 366, p. 01002, 2022.

[15] J. Wang et al., "Comfort-centered design of a lightweight and backdrivable knee exoskeleton," IEEE Robot. Autom. Lett., vol. 3, no. 4, pp. 4265–4272, 2018.

[16] G. Kenneally, A. De, and D. E. Koditschek, "Design principles for a family of direct-drive legged robots," IEEE Robot. Autom. Lett., vol. 1, no. 2, pp. 900–907, 2016.

[17] S. Seok et al., "Design principles for energy-efficient legged locomotion and implementation on the MIT cheetah robot," IEEE ASME Trans. Mechatron., vol. 20, no. 3, pp. 1117–1129, 2015.

[18] V. Kostić et al., "Optimal design and control of multi-motor drive system for industrial application," Tehnicki Vjesnik, vol. 27, no. 6, 2020.

[19] L. Parsa, "On advantages of multi-phase machines," in 31st Annual Conference of IEEE Industrial Electronics Society, 2005. IECON 2005, 2005.

[20] A. Brunner and M. Schrodl, "Mechanical field weakening of a multi-rotor permanent magnet synchronous machine," in 2020 IEEE 9th International Power Electronics and Motion Control Conference (IPEMC2020-ECCE Asia), 2020.

[21] X. Sun et al., "MPTC for PMSMs of EVs with multi-motor driven system considering optimal energy allocation," IEEE Trans. Magn., vol. 55, no. 7, pp. 1–6, 2019.

[22] C. Zhang, S. Zhang, G. Han, and H. Liu, "Power management comparison for a dual-motor-propulsion system used in a battery electric bus," IEEE Trans. Ind. Electron., vol. 64, no. 5, pp. 3873–3882, 2017.

[23] Y. Amano, R. Hibino, M. Sugai, T. Kano, and A. Ishiguro, "A design method of multi-motor system by distributed cooperative control," Trans. Soc. Instrum. Control Eng., vol. 56, no. 11, pp. 521–530, 2020.

[24] T. Saito, K. Hoshiba, Y. Sugahara, and Y. Takeda, "Light weight geared actuator utilizing the drive redundancy," in Mechanisms and Machine Science, Cham: Springer International Publishing, 2022, pp. 246–254.

[25] M. J. Kochenderfer and T. A. Wheeler, Algorithms for optimization. London, England: MIT Press, 2019.

[26] Universal Robots, "UR10e datasheet," 2022. [Online]. Available: https://www.universal-robots.com/media/1807466/ur10e-rgb-fact-sheet-landscape-a4-125-kg.pdf

[27] Maxon, "Product Range 2024/25," 2024. [Online]. Available: https://online.flippingbook.com/view/1042987/

[28] R. G. Budynas and J. K. Nisbett, Shigley's Mechanical Engineering Design, 9th ed. Maidenhead, England: McGraw Hill Higher Education, 2011.